

Received 9 November 2024, accepted 29 November 2024, date of publication 11 December 2024, date of current version 20 December 2024.

Digital Object Identifier 10.1109/ACCESS.2024.3514707



Robust Algorithms for Fitting Q-Factor in the Complex Domain

ANDREW P. GREGORY[®]¹, PETER D. WOOLLIAMS¹, (Member, IEEE), AND STEPHEN M. HANHAM[®]^{2,3}, (Senior Member, IEEE)

¹National Physical Laboratory, TW11 0LW Teddington, U.K.

Corresponding author: Andrew P. Gregory (andrew.gregory@npl.co.uk)

This work was supported in part by U.K. Government's Department for Science, Innovation and Technology through U.K.'s National Measurement Programmes; and in part by the Imperial College London Open Access Fund.

ABSTRACT This paper describes robust vector-fitting algorithms for determining the Q-factor and resonant frequency of spectrally-isolated resonances from frequency-swept S-parameter measurements for both one-port (reflection) and two-port (transmission) systems. It also provides guidance on measurement techniques, and gives measurement examples from the electromagnetic and acoustic domains. These include measurements on a LC resonator (unloaded Q-factor $Q_o \approx 57$), a photonic-crystal resonator ($Q_o \approx 123\,000$) and a superconducting notch resonator ($Q_o \approx 1.5 \times 10^6$). The vector techniques advocated are often advantageous compared to scalar techniques because they are more informative, and in many cases more precise. Among the most common applications is the measurement of dielectric permittivity and loss by resonance at RF and microwave frequencies by using Vector Network Analysers. The algorithms described, however, are applicable more generally to sensing and imaging applications that use vector instrumentation. This is demonstrated by one of the measurement examples, which shows that acoustic Q-factor can be fitted to vibrational data obtained by Resonant Ultrasound Spectroscopy. Open-source software implementations (Python and Matlab) of the algorithms have been made available.

INDEX TERMS Acoustic sensors, dielectric measurement, measurement techniques, microwave measurement, millimeter-wave measurement, network analysers, photonic crystal resonator, Q-factor, resonators, superconducting microwave devices, ultrasonic variables measurement.

I. INTRODUCTION

The applications for measurements of Q-factor and resonant frequency are varied. They include traditional methods of measuring the dielectric permittivity and loss of materials at RF and microwave frequencies [1], [2], and computer-controlled experiments for near-field imaging [3], [4], [5]. Numerous papers describe sensing through measurement of Q-factor and resonant frequency [6]. Many of these describe sensors based on Split-Ring Resonators, and Complementary Split-Ring Resonators [4], [5], [7], [8], [9], [10], [11], [12], [13]. Low-cost miniature VNAs make it possible to find new uses for such devices, particularly for

The associate editor coordinating the review of this manuscript and approving it for publication was Giovanni Angiulli.

biosensing [14], [15]. Piezoelectric actuators can be used to make resonant ultrasound systems for measuring the elastic properties of materials [16]. Microwave measurements on resonators cooled to cryogenic temperatures can be used in studies of the loss mechanisms of superconducting circuits [17]. These can require Q-factors of order 10⁶ to be measured.

This paper describes a collection of robust vector algorithms (NLQFIT) for fitting quality (Q-)factor and resonant frequency to swept measurements of the scattering (S-)parameters of resonant electromagnetic and acoustic systems when resonant modes are spectrally isolated. It supplements a National Physical Laboratory report [18] on Q-factor measurement by using Vector Network Analysers (VNAs). Open-source software implementations

²Department of Materials, Imperial College London, SW7 2AZ London, U.K.

³Department of Electrical, Electronic and Systems Engineering, University of Birmingham, B15 2TT Birmingham, U.K.



(Python and Matlab) of NLQFIT have been made available [18]. An alternative implementation is available from the *scikit-rf* project [19].

The new algorithms use an iterative method of solution that is usually successful even when the swept frequency range is many times broader than the resonance. This simplifies searches for resonances in computer-controlled experiments. Only two initial estimates for fitted values are needed: the approximate resonant frequency and an order-of-magnitude estimate for the Q-factor. These can be obtained from the data. Convergence is not dependent on the accuracy of initial estimates for multiple quantities, which is a limitation for methods that use non-linear fitting routines from a numerical software library [20]. For selected cases, software produced by other authors is available. This has enabled Q-factors fitted by using NLQFIT and by other methods to be compared [18].

The vector techniques for measuring Q-factor that are advocated in this paper are often advantageous compared to scalar techniques because they are more informative, and in many cases more precise [18]. Guidance on experimental techniques for applying them is provided. Five measurement examples that are complementary to those given in reference [18] are given: (i) a comparison of measurements made with high-specification and low-cost VNAs, (ii) a VNA measurement on a low-Q reflection resonator connected via a long cable, (iii) a measurement by Resonant Ultrasound Spectroscopy, (iv) simultaneous measurements by reflection and transmission on a high-Q photonic crystal resonator, and (v) a measurement on a superconducting notch resonator at cryogenic temperature.

A. LITERATURE SURVEY

Q-factor and resonant frequency can be obtained from swept S-parameter data by fitting in the complex plane [21], [22], [23], [24], [25], [26], scalar fitting [27], [28], and by circle fitting [29]. Petersan & Anlage [30], and Bartley & Begley [31] present experimental comparisons between these methods. Q-factors fitted by these methods can show significant differences. The reasons for this are outlined in a more detailed literature survey given in reference [18, Section 1.3].

Methods for fitting in the complex plane, the subject of this paper, are described in a number of papers. Inoue et al. [25] used a linear solution for measurement by transmission in which leakage signal that bypasses the resonator is small enough to neglect. Cox & Jones [26] use a non-linear least-squares fitting routine from a standard library. Kajfez and his co-workers produced several publications [21], [22], [23] in the years after VNAs first became available. These fit Q_L as a complex value, but discard the imaginary part. Q-factors obtained by using Kajfez's QZERO compiled program are in good agreement [18, Table 2] with NLQFIT6 — the equivalent algorithm described in this paper.

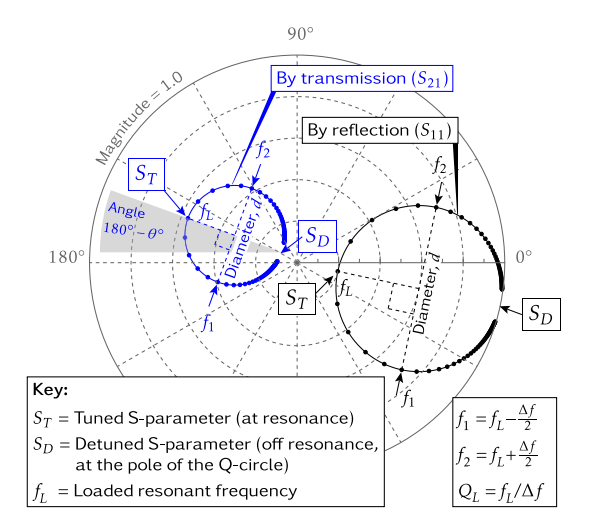


FIGURE 1. S-parameter data for reflection and transmission resonances plotted as a function of frequency on the complex plane. The data was calculated by using equation (1). Phase delays caused by connecting cables are assumed to be zero. Note that couplings are usually chosen to give diameter $d \approx 0.01$ (i.e. smaller than shown) for measurement by transmission, and 0.1 < d < 1.0 for measurement by reflection.

B. GENERAL PRINCIPLES

Resonance equations can be obtained from equivalent-circuit models [18]. For both transmission and reflection resonators that have Q-factor $\gtrsim 100$ and lossless coupling, the complex S-parameter at a frequency f is given by a bilinear transform [22], [24]

$$S(f) = S_D + d \frac{e^{j\theta}}{1 + jQ_L t},$$
equiv.
circuit

in which the fractional offset frequency t is given by

$$t = 2\frac{f - f_L}{f_L}. (2)$$

The symbols Q_L and f_L represent the *loaded* (indicated) Q-factor and resonant frequency, respectively. Other symbols are explained in Fig. 1, which also shows plots of S-parameters as a locus of frequency. Circular responses known as Q-circles are obtained because it is a property of bilinear transforms to map straight lines to arcs on the complex plane by [32]. It is often the case that there are significant mismatches associated with resonator couplings which have a first-order effect on measurements by reflection. In a narrowband approximation these can be described by an additional bilinear transformation. Resonances, however, still appear as Q-circles because the bilinear transform of a bilinear transform is another bilinear transform [22].

Calibrating a VNA with impedance standards defines the positions of *phase reference planes*. For an uncalibrated VNA these are at an unknown location, but are usually close to the front panel connectors of the instrument. Cables between the phase reference planes of the VNA and the resonator, as shown in Fig. 2, are referred to as *uncalibrated lines*. The total physical length of uncalibrated lines is represented



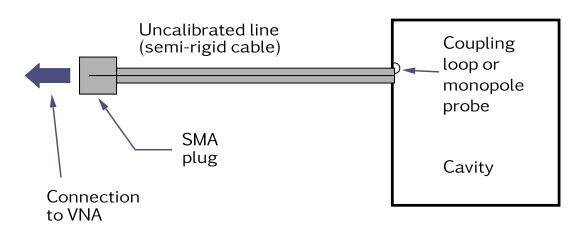


FIGURE 2. One-port cavity with coupler made from semi-rigid coaxial cable.

here by ℓ . Uncalibrated lines cause phase delay, may cause significant attenuation, and will be mismatched unless the 50 Ω characteristic impedance of the VNA ports is maintained throughout. If mismatches are small enough to neglect, the measured S-parameters of resonators that are connected via uncalibrated lines can to an approximation be described by

$$S_a(f) = \alpha(f) e^{-j\phi} e^{-j\Delta\phi} \left[S_D + d \frac{e^{j\theta}}{1 + iO_I t} \right]$$
 (3)

where $\alpha(f)$ is a real valued quantity that describes attenuation in the uncalibrated lines. In the narrow frequency range used for measuring resonances, it is normally sufficient to assume that $\alpha(f)$ has the constant value $\alpha(f_L)$ measured at (or close to) resonance. The phase terms ϕ and $\Delta\phi$ are given by

$$\phi = 2\pi \, \bar{l} \, v f_L / c \tag{4}$$

and

$$\Delta \phi = 2\pi \, \bar{l} \, v \left(f - f_L \right) / c \tag{5}$$

in which c is the velocity of light in a vacuum, v is the velocity factor of the uncalibrated lines (for coaxial cables with solid dielectric $v \simeq \sqrt{\epsilon_r}$ where ϵ_r is the real part of the dielectric permittivity) and

$$\bar{l} = \begin{cases} \ell, & \text{transmission} \\ 2\ell, & \text{reflection.} \end{cases}$$
 (6)

 $\Delta\phi$ represents a frequency-dependent phase delay which is significant because it modifies the shape of the Q-circle, especially if the Q-factor is low. Prior to fitting Q-factor, it is recommended that cables are de-embedded from the measured S-parameter data. If the exact value of \bar{l} is not known, which is generally the case, an estimate should be used. $\Delta\phi$ is then reduced to

$$\Delta \phi = 2\pi \, \delta \bar{l} \, v \left(f - f_L \right) / c \tag{7}$$

where $\delta \bar{l}$ is the error in the estimate of \bar{l} . The rotated detuned S-parameter S_V is given by

$$S_V = S_D e^{-j\phi}. (8)$$

A calibrated value for the Q-circle diameter is required if an estimate of the *unloaded* Q-factor (Q_o) is needed (Section III-D). This should consider attenuation in uncalibrated lines, and the calibration state of the VNA (i.e. calibrated or not calibrated).

Typically, input/output couplers form an integral part of resonators, as shown in Fig. 2. An alternative resonator type, termed a *notch resonator*, uses reactive coupling between a propagating wave in a waveguide, and a one-port resonator that becomes low-impedance at resonance.

Requirements for the most common measurement techniques are discussed below.

1) MEASUREMENT BY TRANSMISSION

VNAs are sensitive instruments, which enables resonances in cavities [1], parallel LC-circuits [2] etc. to be observed by transmission even if weak couplings are used. Weak coupling implies that $Q_o \approx Q_L$ because the loading effect of external circuits on resonances is reduced. Moreover, unless there is excessive noise, measurement precision is usually improved with weak coupling. Typically, couplings are adjusted for transmission loss ≈ 40 dB ($d \approx 0.01$) at resonance.

For measurement by transmission, S_V is often referred to as the *leakage vector*. It represents the signal detected by the VNA receiver that has bypassed the resonator as a result of unwanted couplings between cables, inside the VNA, or directly between the coupling loops or probes of cavity resonators (also known as crosstalk). Coefficients fitted by NLQFIT account for leakage on the asssumption that it occurs predominantly in the locality of the resonator.

Scalar measurements of |S(f)| as a function of frequency yield the familiar Lorentzian [33] if $|S_V| \ll d$. These have the advantage that measurements are unaffected by phase delay in uncalibrated lines, but if there is significant leakage an asymmetric response is obtained [18, Figure 2]. Moreover, random fluctuations of complex S-parameter data manifest themselves as the noise floor of scalar measurements. Algorithms for fitting Q-factor to scalar transmission-coefficient data can be adapted to fit additional coefficients that describe the effects of leakage and the noise floor on the shapes of resonances [28].

2) MEASUREMENT BY REFLECTION

Q-factor measurements by reflection are typically made with the coupling adjusted for strong *undercoupling* (0.1 < d < 1). Measurements can be made with Q-circle diameters as small as d = 0.01, in which case the Q-circle is a very small arc at the edge of the polar chart [18]. This is not ideal, however, as the effect of noise is increased, and iterative methods of obtaining Q-factor are less likely to be successful. *Overcoupling* (i.e. with d > 1.0) is not ideal either, as resonances tend to have poor shape [18].

A consequence of strong coupling into a 50Ω VNA is that Q_L is significantly lower than Q_o . The steps required to estimate Q_o from a fit to complex S-parameter data are outlined in Section III-D2. Using a calibrated VNA improves measurement accuracy (Section III-A), but it is possible to estimate Q_o from uncalibrated measurements. If scalar instrumentation is used [27], [34], an additional measurement to remove ambiguity between overcoupled and undercoupled



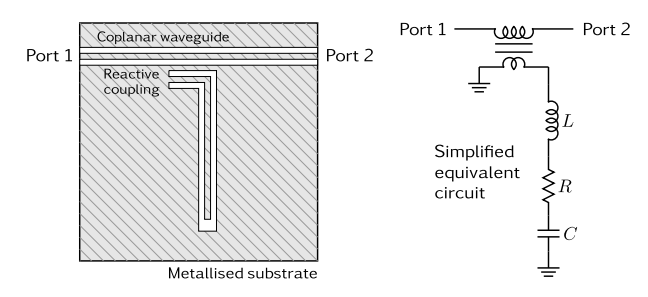


FIGURE 3. Hanger-mode notch resonator and simplified equivalent circuit.

values of Q_o may be required. For vector methods, there is no such ambiguity.

3) FOR A NOTCH RESONATOR BY TRANSMISSION

If a coplanar waveguide is placed in close proximity to a resonant circuit [7], [35], reactive coupling (predominantly inductive) can cause energy to be absorbed at resonance, resulting in a notch in $|S_{21}|$. Strong coupling (Q-circle $d \gtrsim 0.1$) is needed to give the best measurement accuracy. The so-called *hanger mode* configuration (Fig. 3) is suitable for low-temperature measurements made in the inaccessible environment of a cryostat [17], [29] because Q_o can be estimated without additional calibration or normalisation measurements (Section III-D3). Very high Q-factors (e.g. $Q_o > 10^6$) can be obtained for superconducting resonators. The Q-circles of hanger-mode resonators are often pivoted around the fitted value of the detuned transmission coefficient, S_V . This has the effect of making the notch in $|S_{21}|$ asymmetric. Reference [36] explains this phenomenon by using extended equivalent-circuits that represent features at the input and output ports which are not identical; wire-bonded connections that have differing inductance for

A notch resonance in $|S_{21}|$ can also be obtained from a planar circuit fabricated on a substrate with coupling via a microstrip placed on the opposite surface [8], [13]. This configuration normally has a low Q-factor and an asymmetric notch. Q-factors fitted by using the algorithms described in this article will therefore be subject to error. Enhanced equivalent circuits or full-wave numerical simulation techniques [13] provide a more precise description. The resonant modes of a *dielectric resonator* (e.g. a cylinder of low-loss dielectric) coupled with microstrip also appear as notch resonances [37]. Typically, some of these are well-shaped and therefore suitable for characterisation by Q-factor measurement.

II. NLQFIT FITTING ALGORITHMS

The process of fitting to a swept measurement of S_{11} , S_{21} , S_{22} or S_{12} begins by de-embedding the total length of uncalibrated lines according to an estimated value. The resulting data is stored in a one-dimensional vector $S \equiv S_1 \cdots S_N$, where N is the number of frequency points in the sweep.

In the simplest case, in which the error $\delta \bar{l}$ in the estimated length of uncalibrated line is small enough to neglect, (3) reduces to a bilinear transform. To allow for the possibility that the VNA is uncalibrated or $\alpha(f_L)$ is unknown, this can be written in the more generalised form

$$S = \frac{a't + ja''t + b' + jb''}{1 + jQ_L t} \bigg|_{\Delta\phi = 0}$$
 (9)

in which the coefficients a' etc. are real-valued. The calibrated Q-circle parameters S_V and d can be calculated from these coefficients by reference to (3) if the VNA is calibrated and $\alpha(f_L)$ has been determined.

The difference between the value calculated with (9), and the data S for the ith frequency is given by

$$r_i = S_i - \frac{a't_i + ja''t_i + b' + jb''}{1 + jQ_L t_i}.$$
 (10)

To obtain the six coefficients that give a weighted minimisation of $\Sigma |r_i|^2$, a two step process is used; a partial solution (the "initial fit") followed by an optimisation.

This algorithm is referred to as NLQFIT6. Versions of the optimisation step that fit seven and eight fitted coefficients are also described in this paper (see Table 1 for details).

For typical microwave resonators [1], the most suitable algorithms for measurement by transmission and reflection are usually NLQFIT6 and NLQFIT7 respectively. The reasons for this are outlined in Table 1.

TABLE 1. NLQFIT algorithms.

NLQFIT6	Six real-valued coefficients $(m_1 \dots m_6)$ are fitted. It is assumed that uncalibrated lines are de-embedded with sufficient accuracy to ensure that the Q-circle is undistorted. Modelling [18, Section 3.3.1] shows that NLQFIT6 is suitable for measurements on two-port transmission resonators with low leakage $(S_D \ll d)$ provided that $\delta \overline{l} \lesssim \lambda Q_L/180$ (where λ is the wavelength in the uncalibrated lines at the resonant frequency). Resonators of all types that have a very high Q-factor, in superconducting systems for example, can also be fitted by NLQFIT6.
NLQFIT7	Seven real-valued coefficients $(m_1 \dots m_7)$ are fitted. This algorithm is typically used for measurements on reflection and notch resonators. For these, significant error results if only six coefficients are fitted unless the de-embedded length of uncalibrated lines is sufficiently precise (see modelled results in reference [18, Section 3.3.2]). NLQFIT7 avoids such error by determining $\delta \bar{l}$ through the fit.
NLQFIT8	Eight real-valued coefficients $(m_1 ldots m_6, m_8, m_9)$ are fitted. This algorithm can be used for measurements on two-port resonators by transmission when the leakage vector has a linear dependence on frequency [18].

A. INITIAL FIT OF 5 COEFFICIENTS

First (10) is re-written in the form

$$r_i = y_i S_i - y_i \left[b' + jb'' + (a' + ja'' - jQ_L S_i) t_i \right]$$
 (11)

where the complex quantity y_i is given by

$$y_i = \frac{1}{1 + \mathrm{j}Q_L t_i}.\tag{12}$$



If an estimate of f_L is available, the five remaining coefficients (a', a'', b', b'') and Q_L can be fitted by a stable, non-iterative, linear least-squares method. The values y_i appear in every term in (11) and so it may be deduced that $|y_i|^2$ are weighting factors in the minimisation of $\sum |r_i|^2$. It can be sufficient to assume all $|y_i| = 1$, but if they are calculated by using an estimate for Q_L , convergence in the next part of the process (the optimisation) can be improved. The estimate of f_L can be obtained from the measured data by a simple search for the maximum or minimum magnitude according to the type of resonance. In unweighted form, (11) can be represented by the equation

$$\begin{bmatrix} \operatorname{real}(r_{1}) \\ \vdots \\ \operatorname{real}(r_{N}) \\ \operatorname{imag}(r_{1}) \\ \vdots \\ \operatorname{imag}(r_{N}) \end{bmatrix} = \boldsymbol{G} - \boldsymbol{M} \begin{bmatrix} a' \\ a'' \\ b' \\ b'' \\ Q_{L} \end{bmatrix}$$
(13)

where G is a column vector, M is a matrix, and N is the number of frequencies. The weighted solution [38] is given by

$$\begin{bmatrix} a' \\ a'' \\ b' \\ b'' \\ Q_I \end{bmatrix} = C^{-1} q$$
 (14)

in which

$$\boldsymbol{C} = \boldsymbol{M}^T \boldsymbol{P} \boldsymbol{M} \tag{15}$$

and

$$q = M^T PG \tag{16}$$

where the square matrix P is given by

$$\mathbf{P} = \text{Diag} \begin{pmatrix} \begin{bmatrix} |y_1|^2 \\ \vdots \\ |y_N|^2 \\ |y_1|^2 \\ \vdots \\ |y_N|^2 \end{bmatrix} . \tag{17}$$

A linear-equation solver from a numerical software library can be used to solve (14). Even though f_L is not optimised, the solution is useful because it provides initial estimates for an iterative optimisation that fits all of the coefficients required to describe resonances.

B. OPTIMISATION OF 6 FITTED COEFFICIENTS (NLQFIT6)

For measurement by transmission on resonators that have low leakage ($|S_D| \ll d$), $\Delta \phi$ is usually not large enough to have a significant bearing on the fitted Q-factor [18, Section 3.3.1]. It is therefore sufficient to consider only the six coefficients of (10). An iterative optimisation is obtained by using the

gradient-descent method. The five coefficients (14) and estimated f_L are used as initial values.

A change of variables yields the model equation

$$r_i = S_i - [m_1 + jm_2 + (m_3 + jm_4)y_i]$$
 (18)

in which the six real valued coefficients are defined by

$$m_{1} = a''/m_{5} m_{2} = -a'/m_{5}$$

$$m_{3} = b' - m_{1} m_{4} = b'' - m_{2}$$

$$m_{5} = Q_{L} m_{6} = f_{lwst}Q_{L}/f_{L}$$

$$y_{i} = \frac{1}{1 + jQ_{L}t_{i}} = \frac{1}{1 + 2j\left(\frac{m_{6}f_{i}}{f_{lwst}} - m_{5}\right)}.$$
(19)

The lowest frequency $f_{\rm lwst}$ of the measured trace is used as a convenient scaling factor to ensure that m_6 is unitless, otherwise the matrix equation that must be solved can become badly scaled. Changes Δm_k in m_k (for k=1...6) that minimise the summed squares of the real and imaginary parts of e_i in (20) are found by using a weighted linear-least-squares fit similar to that described in Section II-A for solution of (13). Then all m_k are updated ($m_k \rightarrow m_k + \Delta m_k$). The process is repeated until convergence is obtained. The values of y_i must be re-calculated in each iterative loop using the latest values of f_L and Q_L . The equation for e_i is

$$\begin{bmatrix} \operatorname{real}(e_{1}) \\ \vdots \\ \operatorname{real}(e_{N}) \\ \operatorname{imag}(e_{1}) \\ \vdots \\ \operatorname{imag}(e_{N}) \end{bmatrix} = \begin{bmatrix} \operatorname{real}(r_{1}) \\ \vdots \\ \operatorname{real}(r_{N}) \\ \operatorname{imag}(r_{1}) \\ \vdots \\ \operatorname{imag}(r_{N}) \end{bmatrix} - \boldsymbol{M} \begin{bmatrix} \Delta m_{1} \\ \Delta m_{2} \\ \Delta m_{3} \\ \Delta m_{4} \\ \Delta m_{5} \\ \Delta m_{6} \end{bmatrix}$$
(20)

where

$$\mathbf{M} = -\begin{bmatrix} \operatorname{real}\left(\frac{\partial r}{\partial m_{1}}\right)_{1} & \cdots & \operatorname{real}\left(\frac{\partial r}{\partial m_{6}}\right)_{1} \\ \operatorname{real}\left(\frac{\partial r}{\partial m_{1}}\right)_{N} & \cdots & \operatorname{real}\left(\frac{\partial r}{\partial m_{6}}\right)_{N} \\ \operatorname{imag}\left(\frac{\partial r}{\partial m_{1}}\right)_{1} & \cdots & \operatorname{imag}\left(\frac{\partial r}{\partial m_{6}}\right)_{1} \\ \operatorname{imag}\left(\frac{\partial r}{\partial m_{1}}\right)_{N} & \cdots & \operatorname{imag}\left(\frac{\partial r}{\partial m_{6}}\right)_{N} \end{bmatrix} . (21)$$

The partial differentials in (21) can be found analytically without much difficulty. They are evaluated for points $i = 1 \cdots N$ as indicated by suffixes. As reasonably accurate initial estimates are available, rapid convergence is obtained and so few iterations are needed. This being the case it can be sufficient to use a fixed number of iterations. Alternatively, when to exit the iterative loop can be determined from the weighted mean-square deviation between fit and data,

$$\sigma = \sqrt{\frac{\sum_{i=1}^{N} W_i |r_i|^2}{\sum_{i=1}^{N} W_i}}$$
 (22)



where W_i is the weighting factor at the *i*th frequency. Convergence can be said to have occurred when the change in σ between one iterative loop and the next is less than a small fraction (e.g. 10^{-5}) of the magnitude of the largest point in the data array S.

The weighting factors are placed on the diagonal of a square matrix which is incorporated by the least-squares solution of (20) [38]. Initially, they are assumed to be unity for an unweighted fit. The weighting factors proposed in Section III-B can be applied in a repeat of the optimisation.

C. OPTIMISATION OF 7 FITTED COEFFICIENTS (NLQFIT7)

When $|S_D| > |S_T|$, uncalibrated lines cause Q-circles to become distorted [18, Figure 9]. This is especially relevant to measurements by reflection [18, Section 3.3.2] and to measurements on notch resonators, but can also apply to measurements by transmission when there is significant leakage. Accurate de-embedding of uncalibrated lines may be required to avoid substantial error in fits obtained by using NLQFIT6. Moreover, the error becomes larger if Q_L is low-valued or f_L is high-valued.

For some experiments, it is more convenient and accurate to determine the length of uncalibrated line $\delta \bar{l}$ through fitting. This approach is not recommended for transmission measurements when $|S_D| \ll d$ because reliable convergence may not be obtainable.

To fit $\delta \bar{l}$ a modified model equation,

$$r_i = S_i - \left[m_1 + j m_2 + (m_3 + j m_4) y_i \right] e^{j m_7 (f_i - f_L) / f_{lwst}}.$$
(23)

is used. The optimisation algorithm outlined in Section II-B is easily adapted to include the extra fitted coefficient, m_7 . The value of $\delta \bar{l}$ is related to m_7 by

$$m_7 = -\frac{2\pi \ \delta \bar{l} \ v f_{\text{lwst}}}{c}.$$
 (24)

D. OPTIMISATION OF 8 FITTED COEFFICIENTS (NLQFIT8)

Sometimes the shape of transmission resonances can be affected by frequency dependence of the leakage vector [18, Section 4.5]. This can occur when one resonance sits on the "tail" of another. It is straightforward to adapt the optimisation (Section II-B) to include extra coefficients m_8 and m_9 , using the model equation

$$r_i = S_i - \left[m_1 + j m_2 + (m_8 + j m_9) t_i + (m_3 + j m_4) y_i \right].$$
(25)

In the first iterative loop of the optimisation, it can be assumed that $m_8 = m_9 = 0$.

III. EXPERIMENTAL METHOD

A. IS IT NECESSARY TO CALIBRATE THE VNA?

For weakly-coupled two-port resonators measured by transmission, it is found that calibrated measurements of the loaded Q-factor Q_L do not differ significantly

[18, Table 2] from uncalibrated ones made with the VNA's factory correction [18, Section 3.2]. Moreover, the unloaded Q-factor, Q_o , is to an approximation the same as Q_L . If needed, a more traceable and accurate value of Q_o can be obtained by following the process described in Section III-D. This requires an additional measurement to determine a scalar normalisation factor if the VNA is uncalibrated, or $\alpha(f_L) \not\approx 1$,

For measurement by reflection a calibration is recommended as it significantly reduces measurement uncertainties. This is because uncorrected mismatches have a first-order effect [39]. Evidence for this is given in [18, Table 6], which shows that calibrating the VNA improves the consistency of measurements made with varying frequency spans. Where possible, the calibration reference plane should be positioned close to the resonator. Formulae given in Section III-D allow an estimate for Q_o to be obtained from the fitted solution without additional measurements.

Low-temperature transmission measurements on notch resonators in cryostats typically use long and attenuating cable connections that have the incidental effect of suppressing multiple reflections. A VNA calibration in the environment of a cryostat is not easy to obtain, but Q_o can be estimated from uncalibrated measurements by methods described in Sections III-D3 and V-E. At room-temperature, at which notch resonators have comparatively low Q-factor, calibrating the VNA is likely to improve the accuracy of Q-factor measurements significantly. Where this is not possible, inserting attenuators (pads) at each port may give improved accuracy.

B. WEIGHTING BY RATE OF ANGULAR PROGRESSION

If the measured frequencies are equally spaced (i.e. a linear sweep is used), the spacing of points on the Q-circle is greatest near the resonant frequency. Weighting factors can be calculated from the rate of angular progression of frequency around the Q-circle to prevent the "tails" of the resonance having disproportionate effect [18]. They are applied in a repeat of the optimisation step (Section II-B, II-C or II-D). Weighting factors are calculated as a function of frequency by using

$$W_{i} = \frac{1}{\left[\frac{2Q_{L}(f_{i} - f_{L})}{f_{L}}\right]^{2} + 1} . \tag{26}$$

The weighting matrix referred to in Section II-B is given by

$$\mathbf{P} = \operatorname{Diag} \left(\begin{bmatrix} W_1 \\ \vdots \\ W_N \\ W_1 \\ \vdots \\ W_N \end{bmatrix} \right). \tag{27}$$



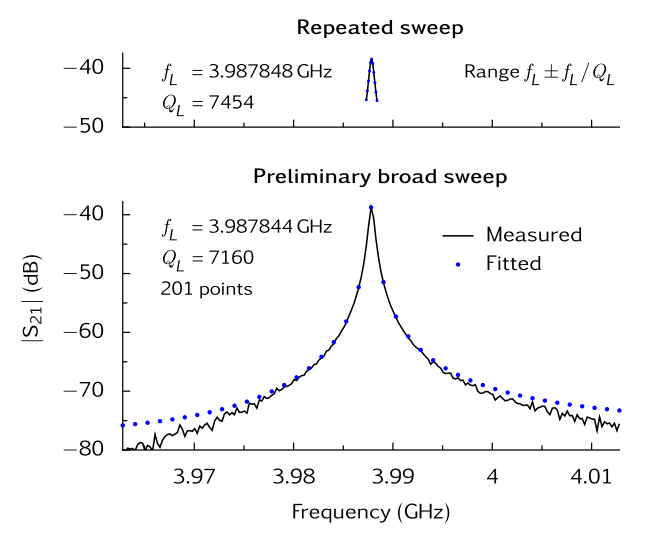


FIGURE 4. Optimisation of the frequency range for a transmission measurement of Q-factor.

C. OPTIMISING THE SWEPT FREQUENCY RANGE

The fitting process described in this paper can usually provide a robust solution even when the swept frequency range is much greater than the width of the resonance Δf (refer to Fig. 1). This can be useful when the resonance frequency is subject to large variation, or when it is desired to observe rapid changes during chemical reactions [40]. Nevertheless, for best accuracy a narrow sweep centred on the resonance is required. This is because (i) the models used are based on narrowband approximations, (ii) Q-factor is defined at the resonant frequency and (iii) the effect of other nearby resonances is reduced. The sweep range for this measurement used by the authors is typically $f_L - f_L/Q_L$ to $f_L + f_L/Q_L$. The corresponding Q-circle seen on a polar plot is an arc that is approximately 70% of a full circle. Suitable values for f_L and Q_L can be obtained by fitting to a preliminary measurement made over a broad frequency-range, as shown in Fig. 4.

D. ESTIMATION OF UNLOADED Q-FACTOR (Q_0)

 Q_o is the Q-factor that would be obtained if the resonator were uncoupled from external circuits (e.g. $50\,\Omega$ VNA and cables). In other words, Q_o describes dissipation by the resonator (assuming it is a closed structure that cannot radiate). The alternative term *internal Q-factor* (Q_i) is sometimes used. Formulae for estimating Q_o are summarised in Table 2. All of these require the calibrated value d of the diameter of the Q circle. Measurements on reflection and notch resonators are normally made with strong coupling, so Q_o is significantly greater than Q_L . Two-port resonators, such as cavities, are normally measured by transmission with weak coupling $(d \approx 0.01)$, which implies that Q_o is only fractionally larger than Q_L . The unusual case of a two-port resonator with strong coupling is discussed in Section V-D.

TABLE 2. Formulae for estimating unloaded Q-factor.

By transmission (assumes that the coupling factors at the two ports are similar).	$Q_o = \frac{Q_L}{1 - d}$	[18]
By reflection (not valid for cavities that are coupled with large loops [18], [22]).	$Q_o = Q_L (1+eta)$ where the coupling factor $eta = rac{1}{rac{2}{d}-1}$	[22]
By transmission for a notch resonator. Simplifies to $Q_o = Q_L/(1-d)$. For asymmetric planar-circuit resonators see the discussion in Section III-D3.	$Q_o = Q_L (1+eta)$ where the coupling factor $eta = rac{1}{rac{1}{d}-1}$	[37], [41]

The calibrated diameter of the Q-circle is given by

$$d = A|m_3 + \mathbf{j}m_4| \tag{28}$$

where A is a real-valued scaling factor that is assumed not to vary with frequency. If the VNA is calibrated and the uncalibrated lines are non-attenuating then A=1.

Some specific details associated with each type of measurement are presented below.

1) BY TRANSMISSION

A "thru" connection in place of the resonator allows A to be determined by measurement if the VNA is uncalibrated $(A=1/|S_{21}|)$. The attenuation of the soldered-in semirigid cables that are often used to make connections to cavity resonators is not usually significant (i.e. $\alpha(f_L) \approx 1$). If necessary, such attenuation can be accounted for by either (i) estimating $\alpha(f_L)$ from measurements by reflection (see examples in Section V-D and in reference [18, Page 43]), or (ii) making the "thru" measurement on a piece of semi-rigid cable that has the overall same length and type as those used to make the connections to the cavity.

2) BY REFLECTION

If the coupling loss is low enough to neglect, all of the signal is reflected off-resonance, i.e. $|S_V| = 1$. If the shape of the resonance accords with the model equation (18) or (23), A can therefore be determined from the fitted coefficients. This approach is recommended even if the VNA is calibrated because attenuation in the uncalibrated line is then accounted for. A is given by

$$A = 1/(|m_1 + jm_2|) . (29)$$

A more elaborate method [22] is needed to obtain a reliable estimate of Q_o for cavity resonators with large loop-couplings because the Q-circles are distorted [18, Figure 16] and the



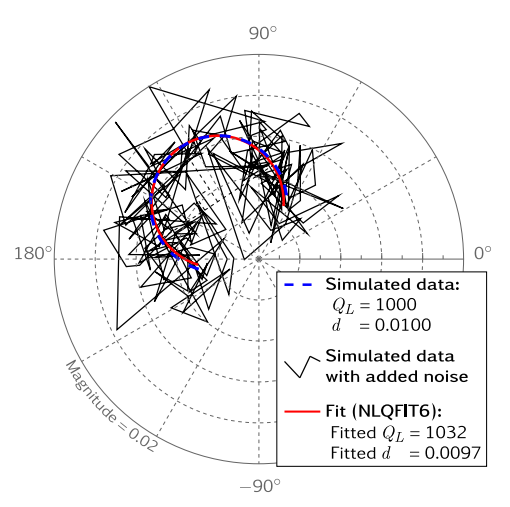


FIGURE 5. A trial used in the study of the effects of simulated noise on Q-factors fitted by using NLQFIT6. The red Q-circle is fitted to transmission data with random noise (normal distribution) added to real and imaginary parts. Shown for the maximum noise ($\sigma = d/5$) for reliable convergence.

parameterised value of S_V is inset from the edge of the polar chart. In this case (29) is inapplicable, but it can be assumed that A=1 if the VNA is calibrated and the attenuation of the uncalibrated line is negligible.

3) FOR A NOTCH RESONATOR BY TRANSMISSION

For this type of resonator, all of the signal is transmitted off-resonance so, assuming that leakage can be neglected, $|S_V| = 1$ and A is given by (29). As remarked in Section I-B3, for asymmetric planar-circuit resonators (e.g. hanger mode) the Q-circle may be pivoted about the fitted value of the detuned point, S_V . This implies that the fitted S_V does not represent the true off-resonance condition according to the equivalent circuit (Fig. 3), and an amended method for estimating Q_o is needed. This topic is further discussed in a measurement example given in Section V-E.

IV. TESTS ON DATA WITH SIMULATED NOISE

 S_{21} data with simulated noise was generated by using computer software for 1000 trials for a resonator with $Q_L = 1000$ and d = 0.01. At each frequency, the simulated noise was derived separately for real and imaginary parts according to a normal distribution with specified standard deviation, σ . One trial is plotted in Fig. 5. Q-factors were fitted to each of the trials by using NLQFIT6, and then averaged. The main purpose of this simulation is investigate how well the algorithm works with noisy data (see the statistical analysis in Table 3). It is found that reliable convergence on a solution for Q_L requires that $\sigma \leq d/5$.

V. MEASUREMENT EXAMPLES

A. A COMPARISON OF MEASUREMENTS OBTAINED WITH

Table 4 shows Q-factor measurements made by transmission with two high specification VNAs and a low-cost handheld

TABLE 3. Q-factors fitted with NLQFIT6 for different levels of noise added to the S_{21} data. The data was obtained by a simulation that used 1000 trials. The nominal values of Q_L and d, were 1000.00 and 0.01 respectively. The simulated S_{21} data had 201 frequency points.

	Statistical analysis of trials		
Simulated S_{21} noise, σ	Average Q_L	$\sigma(Q_L)$	$\sigma_m(Q_L)$
0.00001	999.99	0.35	0.01
0.0001	999.9	3.4	0.1
0.001	1000	33	1
0.002	1011	71	2
>0.002	Convergence not reliable		

 σ = Population standard deviation.

 $\sigma_m = \text{Standard deviation of the mean.}$

TABLE 4. Measurements of Q-factor by transmission on a 1.8 GHz Split-Post Dielectric Resonator (SPDR) made with three uncalibrated VNAs. The results shown are the averages of seven measurements and their standard deviations. The acquisition time ($t_{\rm acq}$) per measurement is also shown

Manufacturer & model	$t_{\rm acq} ({ m sec})$	Fitted data			
Manufacturer & moder		Q_L	σ_{n-1}	Q_o	σ_{n-1}
Hewlett-Packard 8510C	15	16289	4	16463	4
Agilent 8753ES	9	16306	3	16497	4
NanoVNA SAA 2N	36	16304	6	16508	6

instrument (a NanoVNA). The device measured was a 1.8 GHz Split-Post Dielectric Resonator (SPDR) [42] that was wrapped in bubble wrap to minimise thermal drift. The couplers of the SPDR were adjusted to give 40 dB transmission loss. The VNAs were uncalibrated, but measurements on "thru" connections were made to allow Q_o to be estimated (Section III-D1). The data acquisition time $t_{\rm acq}$ is determined by instrument settings (number of points, IF bandwidth etc.). These were chosen to give comparable measurement repeatability for each instrument. The close agreement between the measurements illustrates the potential of low cost VNAs for making accurate sensors.

B. MEASUREMENT OF Q-FACTOR BY REFLECTION WITH A LONG UNCALIBRATED LINE

Fig. 6 shows the polar and magnitude S_{11} traces observed for a loop-coupled LC-resonator that is formed from a single-turn coil shunted by a capacitor. The initial fit (Section II-A) and optimised fit obtained with NLQFIT7 (Section II-C) are also shown on both plots. The trace shown on the polar plot has a cardioid shape because the resonator is connected to the VNA via a long cable (length approximately 8λ), and because the Q-factor is low. Differences between the measured and fitted traces are attributable to the low Q-factor [43], inductive overcoupling [18], and to the use of an uncalibrated VNA [18].

When Q_L is low valued it is found that convergence may fail during the optimisation unless the de-embedded length of cable is known accurately (within \pm 0.1 m for this set of data). When the VNA is uncalibrated, the exact position

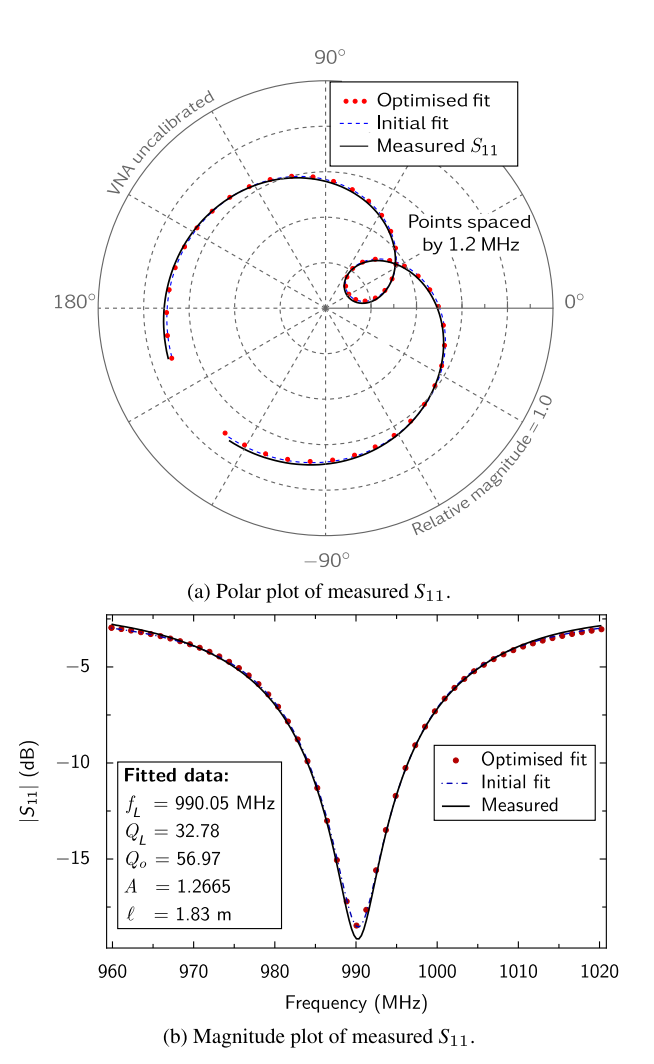


FIGURE 6. Measurement of Q-factor by reflection for a low Q-factor LC-resonator connected by a long cable. The measurements of S_{11} were made with an uncalibrated VNA. Q_o and A are estimated assuming that the effect of mismatches can be neglected. Fitted data was obtained by using NLQFIT7.

of the reference plane for the measurement of phase is not known, which adds further difficulty. A convenient method of estimating the total length of the uncalibrated line is described below. The velocity factor of the cable, ν , is taken to be 1.4 for the data shown in Fig. 6.

1) ESTIMATING THE LENGTH OF THE UNCALIBRATED LINE. For a one-port resonator, the length of uncalibrated line ℓ is easily estimated from a swept measurement of S_{11} . The method used is to replace S_i in (10) by

$$S_i'(\ell) = (S_{11})_i e^{j4\pi \ell v f_i/c}$$
(30)

prior to performing the linear least-squares fit described in Section II-A. An enclosing function is then used to find the value of ℓ that minimises $\Sigma |r_i|^2$ calculated with (11). The authors used an implementation of the Golden Section Search [44] to achieve this.

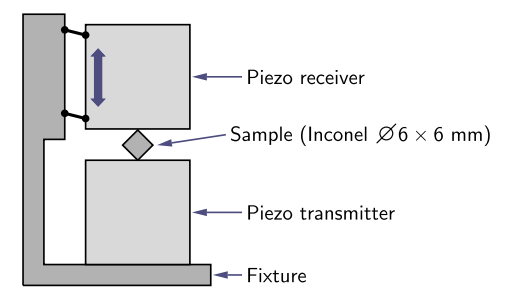


FIGURE 7. Schematic of an instrument for measuring the elastic properties of materials by resonant ultrasound spectroscopy (RUS).

C. THE Q-FACTOR OF AN ULTRASOUND RESONANCE

Resonant Ultrasound Spectroscopy (RUS) is a nondestructive technique for determining the elastic properties of materials by measuring mechanical resonant frequencies [16]. It was developed from seismology and the desire to understand the internal structure of the earth. In the 1990's work was undertaken to develop the mathematical methods for determining the elastic constants of samples that have regular geometric shapes (cylinders and parallelepipeds) from their mechanical resonance spectra. This method is well-suited to measurements on small test samples of metallic and ceramic materials that have low mechanical losses, and are precisely-machined and homogeneous. The number of elastic constants determined through model fitting depends on the expected anisotropy of the sample under test [16], [20], [45]. If required, Q_L can be obtained for magnitude data by using an iterative fitting routine provided that initial estimates of the fitted coefficients are chosen carefully and accurately [20]. In this section, the application NLQFIT6 to RUS data is demonstrated.

A RUS system (model RUS008 manufactured by Alamo Creek Engineering, New Mexico, USA) was used to record the vibrational spectrum of a precision-machined cylinder of wrought Inconel 718 nickel alloy mounted between two piezoelectric tranducers (Fig. 7). Detection is by means of a dual-phase lock-in amplifier. A slow frequency scan was used to avoid ring-down artefacts and obtain very high signal-to-noise ratio spectral data. Q-factor was fitted by means of NLQFIT6. The fitted Q-circle for a resonance at 323 kHz is shown in Fig. 8. The observed leakage, S_V , may be attributed to the signal that propagates between the transducers through the air and through the fixture.

D. UNLOADED Q-FACTOR OF A MILLIMETER-WAVE PHOTONIC CRYSTAL RESONATOR WITH INTEGRATED WAVEGUIDES

A photonic crystal resonator (PCR) is a type of dielectric resonator that utilizes a material with an electromagnetic (EM) bandgap to confine a resonant EM mode [46]. They can achieve very high Q-factors and benefit from small modal volumes and coupling waveguides that can be integrated into the EM bandgap material. One of the difficulties encountered in their Q-factor analysis is the estimation of the coupling



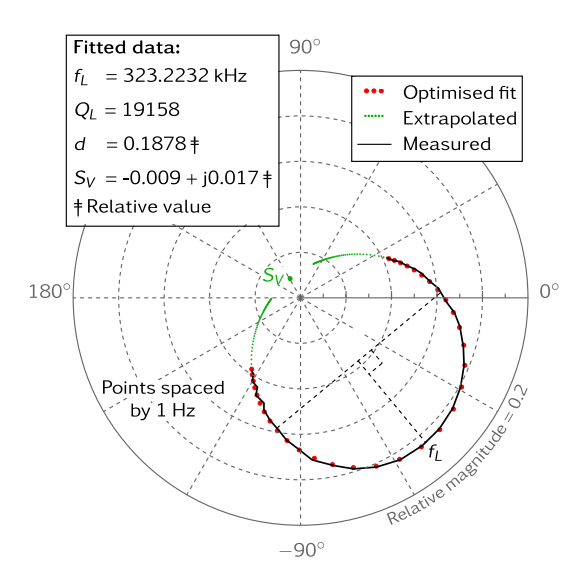


FIGURE 8. Ultrasound resonance fitted with NLQFIT6.

waveguide loss and coupling strength. While these quantities may be calculated in simulation, for measured devices it is more challenging as only the S-parameters of the device may be known with the integrated waveguides functioning as uncalibrated attenuating transmission lines.

As an example, we consider the Q-factor analysis of a millimeter-wave PCR with integrated waveguides, reported in [47]. This PCR was designed for use in an ultra-low phase noise monolithic microwave integrated circuit oscillator and has moderately high coupling strength to optimize the oscillator's phase noise performance [48]. This strength of coupling makes the accuracy of the resonator's unloaded Q-factor highly dependent on an accurate estimation of the coupling strength.

In Fig. 9, we have applied NLQFIT7 to fit the PCR's measured reflection coefficient (S_{11}) and NLQFIT6 to fit the measured forward transmission coefficient (S_{21}). The measuring VNA used coaxial-to-WR19 waveguide adapters on two ports and was calibrated at the waveguide flanges using the two port TRL algorithm. Under strong coupling conditions, a reflection-type estimation of Q-factor is generally considered to have lower uncertainties than a forward transmission-type estimation due to uncertainties associated with the VNA used to perform the measurement [39]. Here we can see that both techniques provide very good fits to the measured data.

As the VNA is calibrated, the coefficients fitted to reflection measurements using NLQFIT7 allow the attenuation of the uncalibrated transmission lines to be characterized. The attenuation was estimated to be $\alpha_1(f_L)=0.86$ and $\alpha_2(f_L)=0.90$ where α_i describes the fitted attenuation for port *i*. The geometric mean of the transmission line attenuation was used for the scaling factor in the transmission Q-factor fitting, i.e. $A=1/\sqrt{\alpha_1(f_L)}\,\alpha_2(f_L)$. Table 5 shows a broad agreement between the reflection and transmission fittings.

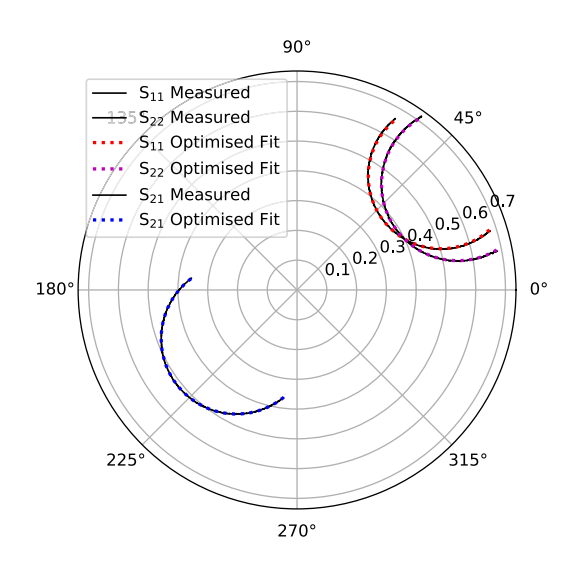


FIGURE 9. Measurement of the unloaded Q-factor of the PCR by reflection and transmission.

TABLE 5. Measurements for the PCR.

	Fitted data		
	f_L (GHz)	Q_L	Q_o
By reflection (S ₁₁)	45.770 660	52 840	122 140
By transmission (S_{21})	45.770 690	52 260	123 000

E. Q-FACTORS OF A SUPERCONDUCTING NOTCH RESONATOR

Table 6 presents Q-factor data fitted to an uncalibrated transmission measurement on a superconducting notch resonator. The resonator, which is of similar design of the resonator to that shown in Fig. 3, was cooled to approximately 10 mK by using a dilution refrigerator [17]. Q-factors obtained by using NLQFIT6 (weighted) and Probst's $resonator_tools$ circlefitting software [29] are shown. For this data, de-embedding the cables does not change the fitted results significantly because Q_L is high-valued. Therefore, for fitting in the complex domain, NLQFIT6 is used in preference to NLQFIT7.

This measurement was discussed previously in reference [18], but is here re-analysed to consider two aspects that are evident on the plotted Q-circle (Fig. 10): pivoting about S_V as described in Section I-B3, and an anomalous deviation from circularity close to the resonant frequency. Both fitting methods are valid when the Q-circle is pivoted.

The presence of an anomaly close to the resonant frequency is unusual; it is more common for anomalies to occur in the "tails" of resonances. Weighting factors reduce the effect of anomalies in the "tails" (Section III-B) but increase the effect of an anomaly close to the resonant frequency. Repeating the NLQFIT6 fit with the largest outliers (10% of points) excluded is observed to result in small changes to the fitted Q_L , f_L and d. The small change in d, however, has a proportionally much greater effect on the estimate for Q_o because the resonator is so strongly coupled.



TABLE 6. Estimates of Q_0 for a superconducting notch resonator fitted to the data shown in Fig. 10.

	Fitting algorithm			
	NLQ	Circle-fit [29]		
	All data	Data without outliers	All Data	
f_L (GHz)	6.072 257	6.072 559	6.072 256	
Q_L	56 020	56 554	56 905	
d	0.9697	0.9755	0.9758	
$r_{ m tc}$	1.0122	1.0126	1.0129	
Q_o (NC)	1 846 783	2 307 799	2 351 434	
Q_o (DCM)			1 515 975	
Q_o (TCM)	1 333 671	1 545 068	1 555 218	

Corrections to Q_o for pivoting of the Q-circle:

NC = No correction.

DCM = Diameter Corrected Method.

TCM = Touching Circle Method.

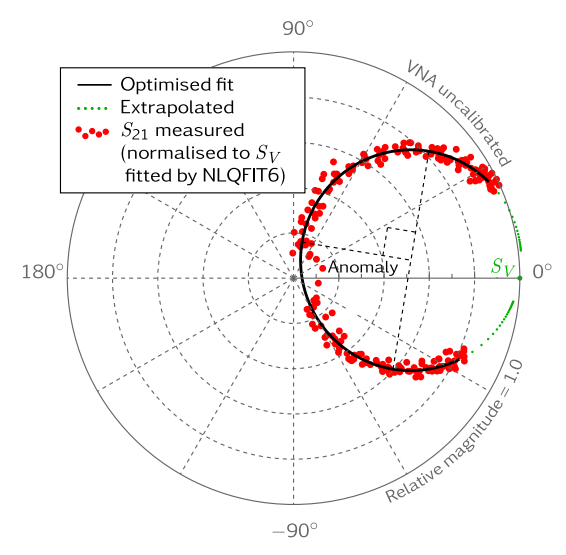


FIGURE 10. Polar plot of fitted and measured S_{21} data for a superconducting notch resonator. The Q-circle for this resonance is pivoted about S_V , and there is an anomaly close to the resonant frequency. There are 239 measured points.

The calculation used for estimating Q_o requires a modification to account for pivoting of the Q-circle. It must also be assumed that leakage signals that bypass the resonator can be neglected. The $resonator_tools$ software implements the diameter-corrected method (DCM) [17], [29], [49]. The authors find that a similar estimate is obtainable from the expression $Q_o = Q_L/(1-d/r_{tc})$. Here, r_{tc} is the radius of the $touching\ circle$ centred at the origin of the polar chart and tangential to the outer edge of the Q-circle. This calculation is based on the assumption that the true off-resonant point (at which the resonator dissipates no energy) is located at the outermost point of the fitted Q-circle. Estimates of Q_o obtained by using NLQFIT6 (with outliers excluded) and $resonator_tools$ (which uses an unweighted fit) are in close agreement.

It should be emphasised that the equivalent circuits on which Q-factor measurements are based assume that resonators have fixed properties. The loss of some materials used in superconducting circuits, however, is dependent on the energy density [17]. In such cases Q-circles may become distorted, which increases measurement uncertainty. Moreover, Q-factors fitted by NLQFIT and circle-fitting algorithms may differ significantly. Convergence failures and spurious fits can also be consequences of such non-linearity.

VI. MEASUREMENT PRECISION

The precision of measurements of Q-factor can be improved by various means that have been described. For example, data can be weighted, and the coupling factor set at an appropriate level for the type of resonator used. Type A (random) uncertainties are readily obtainable by repetition of measurements. The σ_{n-1} data in Table 4 can be taken to be Standard Uncertainties [50], [51]. These, however, are often small compared to Type B (systematic) uncertainties, which are much more difficult to evaluate. Most significantly, Q-factor is determined assuming simple lumped-component equivalent circuits. These are not exact even for a resonator assembled from a capacitor and an inductor because of the distributed nature of wire impedances. For cavity resonators, equivalent circuits are analogies. Therefore, a Type B contribution for *model uncertainty* [52] is needed. There are also significant Type B uncertainty contributions associated with S-parameter measurements and mismatches in uncalibrated lines [53]. These are generally larger (firstorder) for Q-factor measurements by reflection [39] than for transmission (second order). The best guide to the size of the components of the Q-factor uncertainty that are associated with Type B contributions is usually obtained empirically [18].

VII. CONCLUSION

Robust algorithms for fitting Q-factor and resonant frequency in the complex domain have been described. They can be used for measurements on reflection, transmission and notch resonators. The two-step fitting process developed by the authors has been tested in numerous experiments. The information given is sufficient to enable the algorithms to be implemented easily. Guidance on experimental aspects, such as estimation of unloaded Q-factors, is also provided. The measurement examples that have been given demonstrate the usefulness of the algorithms for measuring the radio-frequency and ultrasound properties of materials by resonant methods.

ACKNOWLEDGMENT

The authors would like to thank Jan-Hendrik Buchholz and Indra Ghosh (IMST GmbH, Germany) for performing the VNA measurement of the photonic crystal resonator. They would also like to thank Zahin Ali and Tobias Lindstrom (NPL) for describing their measurements on superconducting resonators and providing data.



SUPPLEMENTARY DATA

Demonstration computer scripts (Python/ Matlab) and example data sets can be obtained from https://doi.org/10.47120/npl.MAT58. An alternative implementation is available from the scikit-rf project https://scikit-rf.readthedocs.io/en/latest/.

REFERENCES

- R. N. Clarke, "Guide to the characterisation of dielectric materials at RF and microwave frequencies," Nat. Phys. Lab., London, U.K., Tech. Rep., 2003
- [2] A. P. Gregory, G. J. Hill, and M. A. Barnett, "Low loss dielectric measurements in the frequency range 1–70 MHz by using a vector network analyser," *Meas. Sci. Technol.*, vol. 32, no. 8, Aug. 2021, Art. no. 085002.
- [3] A. P. Gregory, J. F. Blackburn, T. E. Hodgetts, R. N. Clarke, K. Lees, S. Plint, and G. A. Dimitrakis, "Traceable measurement and imaging of the complex permittivity of a multiphase mineral specimen at micron scales using a microwave microscope," *Ultramicroscopy*, vol. 172, pp. 65–74, Jan. 2017.
- [4] D. Isakov, C. J. Stevens, F. Castles, and P. S. Grant, "A split ring resonator dielectric probe for near-field dielectric imaging," *Sci. Rep.*, vol. 7, no. 1, pp. 1–26, May 2017.
- [5] S. Mukherjee, X. Shi, L. Udpa, S. Udpa, Y. Deng, and P. Chahal, "Design of a split-ring resonator sensor for near-field microwave imaging," *IEEE Sensors J.*, vol. 18, no. 17, pp. 7066–7076, Sep. 2018.
- [6] P. Mehrotra, B. Chatterjee, and S. Sen, "EM-wave biosensors: A review of RF, microwave, mm-wave and optical sensing," *Sensors*, vol. 19, no. 5, p. 1013, Feb. 2019.
- [7] J. D. Baena, J. Bonache, F. Martin, R. M. Sillero, F. Falcone, T. Lopetegi, M. A. G. Laso, J. Garcia-Garcia, I. Gil, M. F. Portillo, and M. Sorolla, "Equivalent-circuit models for split-ring resonators and complementary split-ring resonators coupled to planar transmission lines," *IEEE Trans. Microw. Theory Techn.*, vol. 53, no. 4, pp. 1451–1461, Apr. 2005
- [8] C.-S. Lee and C.-L. Yang, "Complementary split-ring resonators for measuring dielectric constants and loss tangents," *IEEE Microw. Wireless Compon. Lett.*, vol. 24, no. 8, pp. 563–565, Aug. 2014.
- [9] A. Salim and S. Lim, "Review of recent metamaterial microfluidic sensors," Sensors, vol. 18, no. 1, p. 232, Jan. 2018.
- [10] R. Srivastava and S. N. Kale, "Metamaterial inspired resonators as microwave sensors: A review," Eng. Sci. Technol., vol. 2, pp. 28–47, Aug. 2023.
- [11] Z. Xu, Y. Wang, S. Liu, J. Ma, S. Fang, and H. Wu, "Metamaterials with analogous electromagnetically induced transparency and related sensor designs—A review," *IEEE Sensors J.*, vol. 23, no. 7, pp. 6378–6396, Apr. 2023.
- [12] S. P. Chakyar, S. K. Simon, C. Bindu, J. Andrews, and V. P. Joseph, "Complex permittivity measurement using metamaterial split ring resonators," J. Appl. Phys., vol. 121, no. 5, pp. 1–26, Feb. 2017.
- [13] L. Su, J. Mata-Contreras, P. Vélez, A. Fernández-Prieto, and F. Martín, "Analytical method to estimate the complex permittivity of oil samples," *Sensors*, vol. 18, no. 4, p. 984, Mar. 2018.
- [14] A. E. Omer, G. Shaker, S. Safavi-Naeini, H. Kokabi, G. Alquié, F. Deshours, and R. M. Shubair, "Low-cost portable microwave sensor for non-invasive monitoring of blood glucose level: Novel design utilizing a four-cell CSRR hexagonal configuration," *Sci. Rep.*, vol. 10, no. 1, pp. 1–23, Sep. 2020.
- [15] Y. Dong, T. Liu, S. Chen, P. Nithianandam, K. Matar, and J. Li, "A 'two-part' resonance circuit based detachable sweat patch for noninvasive biochemical and biophysical sensing," *Adv. Funct. Mater.*, vol. 33, pp. 1–26, Nov. 2022.
- [16] A. Migliori and J. L. Sarrao, Resonant Ultrasound Spectroscopy: Applications To Physics, Materials Measurements, and Nondestructive Evaluation. Hoboken, NJ, USA: Wiley, 1997.
- [17] C. R. H. McRae, H. Wang, J. Gao, M. R. Vissers, T. Brecht, A. Dunsworth, D. P. Pappas, and J. Mutus, "Materials loss measurements using superconducting microwave resonators," *Rev. Scientific Instrum.*, vol. 91, no. 9, pp. 1–26, Sep. 2020.
- [18] A. P. Gregory, "Q-factor measurement by using a vector network analyser," Nat. Phys. Lab., London, U.K., Tech. Rep. MAT 58, 2021.

- [19] A. Arsenovic, J. Hillairet, J. Anderson, H. Forstén, V. Rieß, M. Eller, N. Sauber, R. Weikle, W. Barnhart, and F. Forstmayr, "Scikit-RF: An open source Python package for microwave network creation, analysis, and calibration," *IEEE Microw. Mag.*, vol. 23, no. 1, pp. 98–105, Jan. 2022.
- [20] B. J. Zadler, J. H. L. Le Rousseau, J. A. Scales, and M. L. Smith, "Resonant ultrasound spectroscopy: Theory and application," *Geophys. J. Int.*, vol. 156, no. 1, pp. 154–169, Jan. 2004.
- [21] D. Kajfez and E. J. Hwan, "Q-factor measurement with network analyzer," IEEE Trans. Microw. Theory Techn., vols. MTT-32, no. 7, pp. 666–670, Jul. 1984.
- [22] D. Kajfez, "Linear fractional curve fitting for measurement of high Q factors," *IEEE Trans. Microw. Theory Techn.*, vol. 42, no. 7, pp. 1149–1153, Jul. 1994.
- [23] D. Kajfez, Q-Factor. Oxford, MA, USA: Vector Fields, 1994.
- [24] K. Leong and J. Mazierska, "Precise measurements of the Q factor of dielectric resonators in the transmission mode-accounting for noise, crosstalk, delay of uncalibrated lines, coupling loss, and coupling reactance," *IEEE Trans. Microw. Theory Techn.*, vol. 50, no. 9, pp. 2115–2127, Sep. 2002.
- [25] R. Inoue, K. Miwa, H. Kitano, A. Maeda, Y. Odate, and E. Tanabe, "Highly accurate and real-time determination of resonant characteristics: Complex linear regression of the transmission coefficient," *IEEE Trans. Microw. Theory Techn.*, vol. 52, no. 9, pp. 2163–2168, Sep. 2004.
- [26] M. G. Cox and H. M. Jones, A Nonlinear Least-Squares Data Fitting Problem Arising Microwave Measurement. London, U.K.: Chapman & Hall, 1990.
- [27] D. Kajfez, "Q-factor measurement with a scalar network analyser," IEE Proc. Microw., Antennas Propag., vol. 142, no. 5, p. 369, Jun. 1995.
- [28] K. J. Coakley, J. D. Splett, M. D. Janezic, and R. F. Kaiser, "Estimation of Q-factors and resonant frequencies," *IEEE Trans. Microw. Theory Techn.*, vol. 51, no. 3, pp. 862–868, Mar. 2003.
- [29] S. Probst, F. B. Song, P. A. Bushev, A. V. Ustinov, and M. Weides, "Efficient and robust analysis of complex scattering data under noise in microwave resonators," *Rev. Sci. Instrum.*, vol. 86, no. 2, Feb. 2015, Art. no. 024706.
- [30] P. J. Petersan and S. M. Anlage, "Measurement of resonant frequency and quality factor of microwave resonators: Comparison of methods," *J. Appl. Phys.*, vol. 84, no. 6, pp. 3392–3402, Sep. 1998.
- [31] P. G. Bartley, "Quality factor determination of resonant structures," in *IEEE Instrum. Meas. Technol. Conf. Proc.*, Dec. 2006, pp. 312–316.
- [32] J. W. Brown and R. V. Churchill, Complex Variables and Applications. New York, NY, USA: McGraw-Hill, 1996.
- [33] D. M. Pozar, Microwave Engineering, 4th ed., Hoboken, NJ, USA: Wiley, 2012.
- [34] R. S. Kwok and J.-F. Liang, "Characterization of high-Q resonators for microwave filter applications," *IEEE Trans. Microw. Theory Techn.*, vol. 47, no. 1, pp. 111–114, Apr. 1999.
- [35] W. Withayachumnankul, K. Jaruwongrungsee, A. Tuantranont, C. Fumeaux, and D. Abbott, "Metamaterial-based microfluidic sensor for dielectric characterization," *Sens. Actuators A, Phys.*, vol. 189, pp. 233–237, Jan. 2013.
- [36] Q.-M. Chen, M. Pfeiffer, M. Partanen, F. Fesquet, K. E. Honasoge, F. Kronowetter, Y. Nojiri, M. Renger, K. G. Fedorov, A. Marx, F. Deppe, and R. Gross, "Scattering coefficients of superconducting microwave resonators. I. transfer matrix approach," *Phys. Rev. B*, vol. 106, no. 21, pp. 1–29, Dec. 2022.
- [37] A. Khanna and Y. Garault, "Determination of loaded, unloaded, and external quality factors of a dielectric resonator coupled to a microstrip line," *IEEE Trans. Microw. Theory Techn.*, vols. MTT-31, no. 3, pp. 261–264, Mar. 1983.
- [38] C. Meyer, Matrix Analysis and Applied Linear Algebra. Philadelphia, PA, USA: SIAM, Jan. 2000.
- [39] D. Kajfez, "Random and systematic uncertainties of reflection-type Q-factor measurement with network analyzer," *IEEE Trans. Microw. Theory Techn.*, vol. 51, no. 2, pp. 512–519, Feb. 2003.
- [40] E. N. Shaforost, N. Klein, S. A. Vitusevich, A. A. Barannik, and N. T. Cherpak, "High sensitivity microwave characterization of organic molecule solutions of nanoliter volume," *Appl. Phys. Lett.*, vol. 94, no. 11, Mar. 2009, Art. no. 112901.
- [41] J. Gao, "The physics of superconducting microwave resonators," Ph.D. thesis, California Inst. Technol., Pasadena, CA, USA, 2008.



- [42] J. Krupka, A. P. Gregory, O. C. Rochard, R. N. Clarke, B. Riddle, and J. Baker-Jarvis, "Uncertainty of complex permittivity measurements by split-post dielectric resonator technique," *J. Eur. Ceram. Soc.*, vol. 21, no. 15, pp. 2673–2676, Jan. 2001.
- [43] A. O. Niedermayer, T. Voglhuber-Brunnmaier, J. Sell, and B. Jakoby, "Methods for the robust measurement of the resonant frequency and quality factor of significantly damped resonating devices," *Meas. Sci. Technol.*, vol. 23, no. 8, Jul. 2012, Art. no. 085107.
- [44] W. H. Press, S. A. Teukolsky, W. T. Vetterling, and B. P. Flannery, *Numer Recipes C.* Cambridge, U.K.: Cambridge University Press, 1992.
- [45] F. F. Balakirev, S. M. Ennaceur, R. J. Migliori, B. Maiorov, and A. Migliori, "Resonant ultrasound spectroscopy: The essential toolbox," *Rev. Sci. Instrum.*, vol. 90, no. 12, pp. 1–26, Dec. 2019.
- [46] J. D. Joannopoulos, S. G. Johnson, J. N. Winn, and R. D. Meade, *Photonic Crystals: Molding Flow Light*. Princeton, NJ, USA: Princeton Univ. Press, 2011
- [47] S. M. Hanham, J.-H. Buchholz, H. Fischer, U. Gollor, J. Lehmke, W. Wischmann, I. Ghosh, E. Lia, B. Walter, F. Bavedila, M. Faucher, A. Gregory, L. Jensen, and R. Follmann, "Low dielectric filling factor millimeter-wave photonic crystal resonator micromachined from NTD high-resistivity silicon," *IEEE Trans. Microw. Theory Techn.*, vol. 72, no. 11, pp. 6601–6612, Nov. 2024.
- [48] E. Lia, I. Ghosh, S. M. Hanham, B. Walter, F. Bavedila, M. Faucher, A. P. Gregory, L. Jensen, J. Buchholz, H. Fischer, U. Altmann, and R. Follmann, "Novel mm-wave oscillator based on an electromagnetic bandgap resonator," *IEEE Microw. Wireless Technol. Lett.*, vol. 33, no. 1, pp. 1–4, Jun. 2023.
- [49] M. S. Khalil, M. J. A. Stoutimore, F. C. Wellstood, and K. D. Osborn, "An analysis method for asymmetric resonator transmission applied to superconducting devices," *J. Appl. Phys.*, vol. 111, no. 5, pp. 1–20, Mar. 2012.
- [50] Evaluation of Measurement Data-Guide To the Expression of Uncertainty in Measurement, document JCGM 100, BIPM, 2008.
- [51] The Expression of Uncertainty and Confidence in Measurement, document M3003, United Kingdom Accreditation Service, 2019.
- [52] Guide To the Expression of Uncertainty in Measurement—Part 6: Developing and Using Measurement Models, document JCGM GUM6, BIPM, 2020.
- [53] D. Kajfez, S. Chebolu, M. R. Abdul-Gaffoor, and A. A. Kishk, "Uncertainty analysis of the transmission-type measurement of Q-factor," *IEEE Trans. Microw. Theory Techn.*, vol. 47, no. 3, pp. 367–371, Mar. 1999.

ANDREW P. GREGORY received the degree from The University of Manchester. In 1984, he joined the National Physical Laboratory, U.K. He has spent most of his career developing methods for measuring the dielectric properties of liquid and solid materials at RF and microwave frequencies.

PETER D. WOOLLIAMS (Member, IEEE) received the degree from Imperial College London. He is currently with the Advanced Engineering Materials Team, National Physical Laboratory, U.K. His research interests include materials testing, 3D printing, and metamaterials.



STEPHEN M. HANHAM (Senior Member, IEEE) received the B.E. and B.Sc. degrees from the University of Western Australia, Perth, WA, Australia, in 2004, and the Ph.D. degree from The University of Sydney, Sydney, NSW, Australia, in 2010. From 2008 to 2010, he was a Research Project Officer, and later, a System Engineer at the Commonwealth Scientific and Industrial Research Organization (CSIRO), Sydney, working in the areas of electromagnetics and antennas,

primarily aimed toward the terahertz band. From 2010 to 2017, he was a Postdoctoral Research Associate and then an Experienced Researcher with the Physics and Materials Departments, Imperial College London, London, U.K., researching terahertz plasmonics, near-field imaging, and liquid sensing. From 2017 to 2024, he was a Senior Birmingham Fellow and an Associate Professor with the Department of Electronic, Electrical and Systems Engineering, University of Birmingham, Birmingham, U.K. He is currently a Senior Lecturer with the Department of Materials, Imperial College London. He has more than 70 publications in scientific journals, international conferences, and book chapters spanning the fields of electronic engineering, physics, and material science. His research interests include terahertz and microwave technologies for sensing applications, most recently metamaterials, plasmonics, nanomaterials, and electromagnetic devices.

. . .